
Intriguing properties of neural networks

Christian Szegedy

Google Inc.

Wojciech Zaremba

New York University

Ilya Sutskever

Google Inc.

Joan Bruna

New York University

Dumitru Erhan

Google Inc.

Ian Goodfellow

University of Montreal

Rob Fergus

New York University

Facebook Inc.

Abstract

Deep neural networks are highly expressive models that have recently achieved state of the art performance on speech and visual recognition tasks. While their expressiveness is the reason they succeed, it also causes them to learn uninterpretable solutions that could have counter-intuitive properties. In this paper we report two such properties.

First, we find that there is no distinction between individual high level units and random linear combinations of high level units, according to various methods of unit analysis. It suggests that it is the space, rather than the individual units, that contains the semantic information in the high layers of neural networks.

Second, we find that deep neural networks learn input-output mappings that are fairly discontinuous to a significant extent. We can cause the network to misclassify an image by applying a certain hardly perceptible perturbation, which is found by maximizing the network's prediction error. In addition, the specific nature of these perturbations is not a random artifact of learning: the same perturbation can cause a different network, that was trained on a different subset of the dataset, to misclassify the same input.

1 Introduction

Deep neural networks are powerful learning models that achieve excellent performance on visual and speech recognition problems [9, 8]. Neural networks achieve high performance because they can express arbitrary computation that consists of a modest number of massively parallel nonlinear steps. But as the resulting computation is automatically discovered by backpropagation via supervised learning, it can be difficult to interpret and can have counter-intuitive properties. In this paper, we discuss two counter-intuitive properties of deep neural networks.

The first property is concerned with the semantic meaning of individual units. Previous works [6, 13, 7] analyzed the semantic meaning of various units by finding the set of inputs that maximally activate a given unit. The inspection of individual units makes the implicit assumption that the units of the last feature layer form a distinguished basis which is particularly useful for extracting semantic information. Instead, we show in section 3 that random projections of $\phi(x)$ are semantically indistinguishable from the coordinates of $\phi(x)$. This puts into question the conjecture that neural networks disentangle variation factors across coordinates. Generally, it seems that it is the entire space of activations, rather than the individual units, that contains the bulk of the semantic information. A similar, but even stronger conclusion was reached recently by Mikolov et al. [12] for word representations, where the various directions in the vector space representing the words are shown to give rise to a surprisingly rich semantic encoding of relations and analogies. At the same time,

the vector representations are stable up to a rotation of the space, so the individual units of the vector representations are unlikely to contain semantic information.

The second property is concerned with the stability of neural networks with respect to small perturbations to their inputs. Consider a state-of-the-art deep neural network that generalizes well on an object recognition task. We expect such network to be robust to small perturbations of its input, because small perturbation cannot change the object category of an image. However, we find that applying an *imperceptible* non-random perturbation to a test image, it is possible to arbitrarily change the network’s prediction (see figure 5). These perturbations are found by optimizing the input to maximize the prediction error. We term the so perturbed examples “adversarial examples”.

It is natural to expect that the precise configuration of the minimal necessary perturbations is a random artifact of the normal variability that arises in different runs of backpropagation learning. Yet, we found that adversarial examples are relatively robust, and are shared by neural networks with varied number of layers, activations or trained on different subsets of the training data. That is, if we use one neural net to generate a set of adversarial examples, we find that these examples are still statistically hard for another neural network even when it was trained with different hyperparameters or, most surprisingly, when it was trained on a different set of examples.

These results suggest that the deep neural networks that are learned by backpropagation have nonintuitive characteristics and intrinsic blind spots, whose structure is connected to the data distribution in a non-obvious way.

2 Framework

Notation We denote by $x \in \mathbb{R}^m$ an input image, and $\phi(x)$ activation values of some layer. We first examine properties of the image of $\phi(x)$, and then we search for its blind spots.

We perform a number of experiments on a few different networks and three datasets :

- For the MNIST dataset, we used the following architectures [11]
 - A simple fully connected network with one or more hidden layers and a Softmax classifier. We refer to this network as “FC”.
 - A classifier trained on top of an autoencoder. We refer to this network as “AE”.
- The ImageNet dataset [3].
 - Krizhevsky et. al architecture [9]. We refer to it as “AlexNet”.
- $\sim 10M$ image samples from Youtube (see [10])
 - Unsupervised trained network with ~ 1 billion learnable parameters. We refer to it as “QuocNet”.

For the MNIST experiments, we use regularization with a weight decay of λ . Moreover, in some experiments we split the MNIST training dataset into two disjoint datasets P_1 , and P_2 , each with 30000 training cases.

3 Units of: $\phi(x)$

Traditional computer vision systems rely on feature extraction: often a single feature is easily interpretable, e.g. a histogram of colors, or quantized local derivatives. This allows one to inspect the individual coordinates of the feature space, and link them back to meaningful variations in the input domain. Similar reasoning was used in previous work that attempted to analyze neural networks that were applied to computer vision problems. These works interpret an activation of a hidden unit as a meaningful feature. They look for input images which maximize the activation value of this single feature [6, 13, 7, 4].

The aforementioned technique can be formally stated as visual inspection of images x' , which satisfy (or are close to maximum attainable value):

$$x' = \arg \max_{x \in \mathcal{I}} \langle \phi(x), e_i \rangle$$

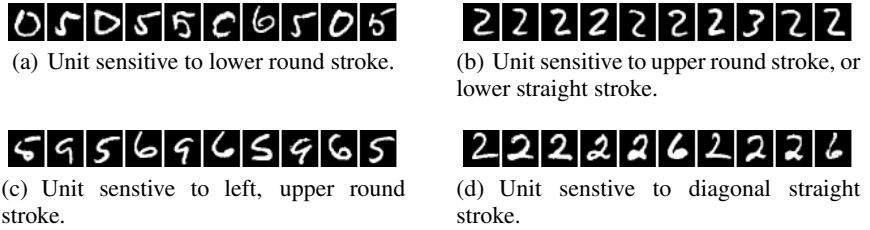


Figure 1: An MNIST experiment. The figure shows images that maximize the activation of various units (maximum stimulation in the natural basis direction). Images within each row share semantic properties.

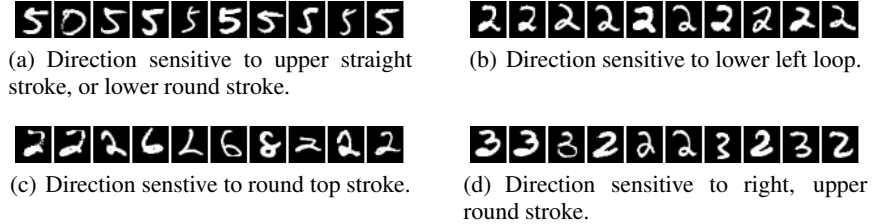


Figure 2: An MNIST experiment. The figure shows images that maximize the activations in a random direction (maximum stimulation in a random basis). Images within each row share semantic properties.

where \mathcal{I} is a held-out set of images from the data distribution that the network was not trained on and e_i is the natural basis vector associated with the i -th hidden unit.

Our experiments show that any random direction $v \in \mathbb{R}^n$ gives rise to similarly interpretable semantic properties. More formally, we find that images x' are semantically related to each other, for many x' such that

$$x' = \arg \max_{x \in \mathcal{I}} \langle \phi(x), v \rangle$$

This suggests that the natural basis is not better than a random basis for inspecting the properties of $\phi(x)$. This puts into question the notion that neural networks disentangle variation factors across coordinates.

First, we evaluated the above claim using a convolutional neural network trained on MNIST. We used the MNIST test set for \mathcal{I} . Figure 1 shows images that maximize the activations in the natural basis, and Figure 2 shows images that maximize the activation in random directions. In both cases the resulting images share many high-level similarities.

Next, we repeated our experiment on an AlexNet, where we used the validation set as \mathcal{I} . Figures 3 and 4 compare the natural basis to the random basis on the trained network. The rows appear to be semantically meaningful for both the single unit and the combination of units.

Although such analysis gives insight on the capacity of ϕ to generate invariance on a particular subset of the input distribution, it does not explain the behavior on the rest of its domain. We shall see in the next section that ϕ has counterintuitive properties in the neighbourhood of almost every point from data distribution.

4 Blind Spots in Neural Networks

So far, unit-level inspection methods had relatively little utility beyond confirming certain intuitions regarding the complexity of the representations learned by a deep neural network [6, 13, 7, 4]. Global, network level inspection methods *can* be useful in the context of explaining classification decisions made by a model [1] and can be used to, for instance, identify the parts of the input which led to a correct classification of a given visual input instance (in other words, one can use a trained

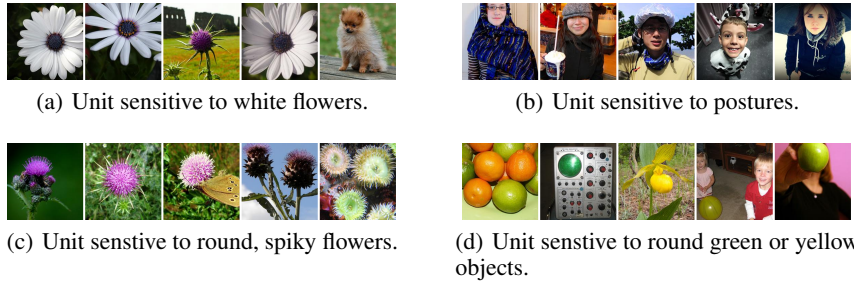


Figure 3: Experiment performed on ImageNet. Images stimulating single unit most (maximum stimulation in natural basis direction). Images within each row share many semantic properties.

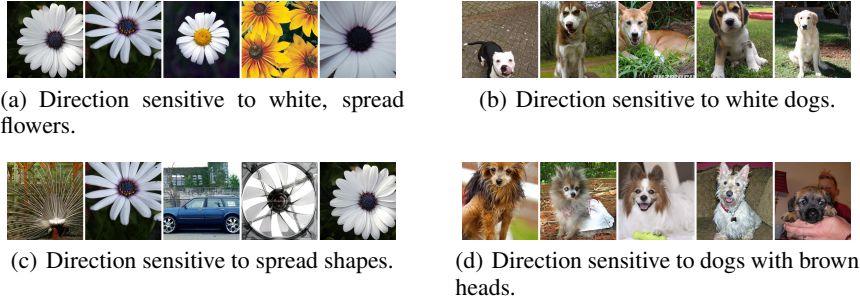


Figure 4: Experiment performed on ImageNet. Images giving rise to maximum activations in a random direction (maximum stimulation in a random basis). Images within each row share many semantic properties.

model for weakly-supervised localization). Such global analyses are useful in that they can make us understand better the input-to-output mapping represented by the trained network.

Generally speaking, the output layer unit of a neural network is a highly nonlinear function of its input. When it is trained with the cross-entropy loss (using the Softmax activation function), it represents a conditional distribution of the label given the input (and the training set presented so far). It has been argued [2] that the deep stack of non-linear layers in between the input and the output unit of a neural network are a way for the model to encode a *non-local generalization prior* over the input space. In other words, it is assumed that is possible for the output unit to assign non-significant (and, presumably, non- ϵ) probabilities to regions of the input space that contain no training examples in their vicinity. Such regions can represent, for instance, the same objects from different viewpoints, which are relatively far (in pixel space), but which share nonetheless both the label and the statistical structure of the original inputs.

It is implicit in such arguments that *local* generalization—in the very proximity of the training examples—works as expected. And that in particular, for a small enough radius $\varepsilon > 0$ in the vicinity of a given training input x , an $x + r$ satisfying $\|r\| < \varepsilon$ will get assigned a high probability of the correct class by the model. This kind of smoothness prior is typically valid for computer vision problems. In general, imperceptibly tiny perturbations of a given image do not normally change the underlying class.

Our main result is that for deep neural networks, the smoothness assumption that underlies many kernel methods does not hold. Specifically, we show that by using a simple optimization procedure, we are able to find adversarial examples, which are obtained by imperceptibly small perturbations to a correctly classified input image, so that it is no longer classified correctly.

In some sense, what we describe is a way to traverse the manifold represented by the network in an efficient way (by optimization) and finding *adversarial examples* in the input space. The adversarial examples represent low-probability (high-dimensional) “pockets” in the manifold, which are hard to efficiently find by simply randomly sampling the input around a given example. Already, a variety of recent state of the art computer vision models employ input deformations during training for

increasing the robustness and convergence speed of the models [9, 13]. These deformations are, however, statistically inefficient, for a given example: they are highly correlated and are drawn from the same distribution throughout the entire training of the model. We propose a scheme to make this process adaptive in a way that exploits the model and its deficiencies in modeling the local space around the training data.

We make the connection with hard-negative mining explicitly, as it is close in spirit: hard-negative mining, in computer vision, consists of identifying training set examples (or portions thereof) which are given low probabilities by the model, but which should be high probability instead, cf. [5]. The training set distribution is then changed to emphasize such hard negatives and a further round of model training is performed. As shall be described, the optimization problem proposed in this work can also be used in a constructive way, similar to the hard-negative mining principle.

4.1 Formal description

We denote by $f : \mathbb{R}^m \rightarrow \{1 \dots k\}$ a classifier mapping image pixel value vectors to a discrete label set. We also assume that f has an associated continuous loss function denoted by $\text{loss}_f : \mathbb{R}^m \times \{1 \dots k\} \rightarrow \mathbb{R}^+$. For a given $x \in \mathbb{R}^m$ image and target label $l \in \{1 \dots k\}$, we aim to solve the following box-constrained optimization problem:

- Minimize $\|r\|_2$ subject to:
 1. $f(x + r) = l$
 2. $x + r \in [0, 1]^m$

The minimizer r might not be unique, but we denote one such $x + r$ for an arbitrarily chosen minimizer by $D(x, l)$. Informally, $x + r$ is the closest image to x classified as l by f . Obviously, $D(x, f(x)) = f(x)$, so this task is non-trivial only if $f(x) \neq l$. In general, the exact computation of $D(x, l)$ is a hard problem, so we approximate it by using a box-constrained L-BFGS. Concretely, we find an approximation of $D(x, l)$ by performing line-search to find the minimum $c > 0$ for which the minimizer r of the following problem satisfies $f(x + r) = l$.

- Minimize $c|r| + \text{loss}_f(x + r, l)$ subject to $x + r \in [0, 1]^m$

This penalty function method would yield the exact solution for $D(X, l)$ in the case of convex losses, however neural networks are non-convex in general, so we end up with an approximation in this case.

4.2 Experimental results

Our “minimum distortion” function D has the following intriguing properties which we will support by informal evidence and quantitative experiments in this section:

1. For all the networks we studied (MNIST, QuocNet [10], AlexNet [9]), for each sample, we have always managed to generate very close, visually hard to distinguish, adversarial examples that are misclassified by the original network (see figure 5 and <http://goo.gl/huaGPb> for examples).
2. *Cross model generalization*: a relatively large fraction of examples will be misclassified by networks trained from scratch with different hyper-parameters (number of layers, regularization or initial weights).
3. *Cross training-set generalization*: a relatively large fraction of examples will be misclassified by networks trained from scratch on a disjoint training set.

The above observations suggest that adversarial examples are somewhat universal and not just the results of overfitting to a particular model or to the specific selection of the training set. They also suggest that back-feeding adversarial examples to training might improve generalization of the resulting models. Our preliminary experiments have yielded positive evidence on MNIST to support this hypothesis as well: We have successfully trained a two layer 100-100-10 non-convolutional neural network with a test error below 1.2% by keeping a pool of adversarial examples a random subset of which is continuously replaced by newly generated adversarial examples and which is mixed into



Figure 5: Adversarial examples generated for AlexNet [9].(Left) is a correctly predicted sample, (center) difference between correct image, and image predicted incorrectly magnified by 10x (values shifted by 128 and clamped), (right) adversarial example. All images in the right column are predicted to be an “ostrich, *Struthio camelus*”. Average distortion based on 64 examples is 0.006508. Please refer to <http://goo.gl/huaGPb> for full resolution images. The examples are strictly randomly chosen. There is not any postselection involved.



Figure 6: Adversarial examples for QuocNet [10]. A binary car classifier was trained on top of the last layer features without fine-tuning. The randomly chosen examples on the left are recognized correctly as cars, while the images in the middle are not recognized. The rightmost column is the magnified absolute value of the difference between the two images.

the original training set all the time. We used weight decay, but no dropout for this network. For comparison, a network of this size gets to 1.6% errors when regularized by weight decay alone and can be improved to around 1.3% by using carefully applied dropout. A subtle, but essential detail is that we only got improvements by generating adversarial examples for each layer outputs which were used to train all the layers above. The network was trained in an alternating fashion, maintaining and updating a pool of adversarial examples for each layer separately in addition to the original training set. According to our initial observations, adversarial examples for the higher layers seemed to be significantly more useful than those on the input or lower layers. In our future work, we plan to compare these effects in a systematic manner.

For space considerations, we just present results for a representative subset (see Table 1) of the MNIST experiments we performed. The results presented here are consistent with those on a larger variety of non-convolutional models. For MNIST, we do not have results for convolutional models yet, but our first qualitative experiments with AlexNet gives us reason to believe that convolutional networks may behave similarly as well. Each of our models were trained with L-BFGS until convergence. The first three models are linear classifiers that work on the pixel level with various weight decay parameters λ . All our examples use quadratic weight decay on the connection weights: $\text{loss}_{\text{decay}} = \lambda \sum w_i^2 / k$ added to the total loss, where k is the number of units in the layer. Three of our models are simple linear (softmax) classifier without hidden units ($\text{FC}10(\lambda)$). One of them, $\text{FC}10(1)$, is trained with extremely high $\lambda = 1$ in order to test whether it is still possible to generate adversarial examples in this extreme setting as well. Two other models are a simple sigmoidal neural network with two hidden layers and a classifier. The last model, $\text{AE}400-10$, consists of a single layer sparse autoencoder with sigmoid activations and 400 nodes with a Softmax classifier. This network has been trained until it got very high quality first layer filters and this layer was **not** fine-tuned. The last column measures the minimum average pixel level distortion necessary to reach 0% accuracy on the training set. The distortion is measured by $\sqrt{\frac{\sum(x'_i - x_i)^2}{n}}$ between the original x and distorted

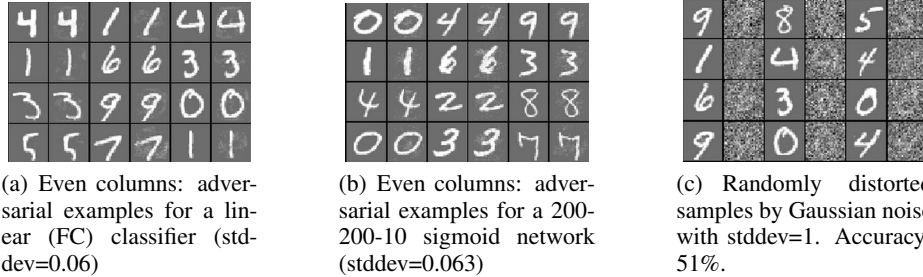


Figure 7: Adversarial examples for a randomly chosen subset of MNIST compared with randomly distorted examples. Odd columns correspond to original images, and even columns correspond to distorted counterparts. The adversarial examples generated for the specific model have accuracy 0% for the respective model. Note that while the randomly distorted examples are hardly readable, still they are classified correctly in half of the cases, while the adversarial examples are never classified correctly.

Model Name	Description	Training error	Test error	Av. min. distortion
FC10(10^{-4})	Softmax with $\lambda = 10^{-4}$	6.7%	7.4%	0.062
FC10(10^{-2})	Softmax with $\lambda = 10^{-2}$	10%	9.4%	0.1
FC10(1)	Softmax with $\lambda = 1$	21.2%	20%	0.14
FC100-100-10	Sigmoid network $\lambda = 10^{-5}, 10^{-5}, 10^{-6}$	0%	1.64%	0.058
FC200-200-10	Sigmoid network $\lambda = 10^{-5}, 10^{-5}, 10^{-6}$	0%	1.54%	0.065
AE400-10	Autoencoder with Softmax $\lambda = 10^{-6}$	0.57%	1.9%	0.086

Table 1: Tests of the generalization of adversarial instances on MNIST.

	FC10(10^{-4})	FC10(10^{-2})	FC10(1)	FC100-100-10	FC200-200-10	AE400-10	Av. distortion
FC10(10^{-4})	100%	11.7%	22.7%	2%	3.9%	2.7%	0.062
FC10(10^{-2})	87.1%	100%	35.2%	35.9%	27.3%	9.8%	0.1
FC10(1)	71.9%	76.2%	100%	48.1%	47%	34.4%	0.14
FC100-100-10	28.9%	13.7%	21.1%	100%	6.6%	2%	0.058
FC200-200-10	38.2%	14%	23.8%	20.3%	100%	2.7%	0.065
AE400-10	23.4%	16%	24.8%	9.4%	6.6%	100%	0.086
Gaussian noise, stddev=0.1	5.0%	10.1%	18.3%	0%	0%	0.8%	0.1
Gaussian noise, stddev=0.3	15.6%	11.3%	22.7%	5%	4.3%	3.1%	0.3

Table 2: Cross-model generalization of adversarial examples. The columns of the Tables show the error induced by distorted examples fed to the given model. The last column shows average distortion wrt. original training set.

x' images, where $n = 784$ is the number of image pixels. The pixel intensities are scaled to be in the range $[0, 1]$.

In our first experiment, we generated a set of adversarial instances for a given network and fed these examples for each other network to measure the proportion of misclassified instances. The last column shows the average minimum distortion that was necessary to reach 0% accuracy on the whole training set. The experimental results are presented in Table 2. The columns of Table 2 show the error (proportion of misclassified instances) on the so distorted training sets. The last two rows are given for reference showing the error induced when distorting by the given amounts of Gaussian noise. Note that even the noise with stddev 0.1 is greater than the stddev of our adversarial noise for all but one of the models. Figure 7 shows a visualization of the generated adversarial instances for two of the networks used in this experiment. The general conclusion is that adversarial examples tend to stay hard even for models trained with different hyperparameters. Although the autoencoder based version seems most resilient to adversarial examples, it is not fully immune either.

Still, this experiment leaves open the question of dependence over the training set. Does the hardness of the generated examples rely solely on the particular choice of our training set as a sample or does this effect generalize even to models trained on completely different training sets?

Model	Error on P_1	Error on P_2	Error on Test	Min Av. Distortion
FC100-100-10: 100-100-10 trained on P_1	0%	2.4%	2%	0.062
FC123-456-10: 123-456-10 trained on P_1	0%	2.5%	2.1%	0.059
FC100-100-10' trained on P_2	2.3%	0%	2.1%	0.058

Table 3: Models trained to study cross-training-set generalization of the generated adversarial examples. Errors presented in Table correpond to original not-distorted data, to provide a baseline.

	FC100-100-10	FC123-456-10	FC100-100-10'
Distorted for FC100-100-10 (av. stddev=0.062)	100%	26.2%	5.9%
Distorted for FC123-456-10 (av. stddev=0.059)	6.25%	100%	5.1%
Distorted for FC100-100-10' (av. stddev=0.058)	8.2%	8.2%	100%
Gaussian noise with stddev=0.06	2.2%	2.6%	2.4%
Distorted for FC100-100-10 amplified to stddev=0.1	100%	98%	43%
Distorted for FC123-456-10 amplified to stddev=0.1	96%	100%	22%
Distorted for FC100-100-10' amplified to stddev=0.1	27%	50%	100%
Gaussian noise with stddev=0.1	2.6%	2.8%	2.7%

Table 4: Cross-training-set generalization error rate for the set of adversarial examples generated for different models. The error induced by a random distortion to the same examples is displayed in the last row.

To study cross-training-set generalization, we have partitioned the 60000 MNIST training images into two parts P_1 and P_2 of size 30000 each and trained three non-convolutional networks with sigmoid activations on them: Two, FC100-100-10 and FC123-456-10, on P_1 and FC100-100-10 on P_2 . The reason we trained two networks for P_1 is to study the cumulative effect of changing the hyperparameters and the training sets at the same time. Models FC100-100-10 and FC100-100-10 share the same hyperparameters: both of them are 100-100-10 networks, while FC123-456-10 has different number of hidden units. In this experiment, we were distorting the elements of the test set rather than the training set. Table 3 summarizes the basic facts about these models. After we generate adversarial examples with 100% error rates with minimum distortion for the test set, we feed these examples to the each of the models. The error for each model is displayed in the corresponding column of the upper part of Table 4. In the last experiment, we magnify the effect of our distortion by using the examples $x + 0.1 \frac{x' - x}{\|x' - x\|_2}$ rather than x' . This magnifies the distortion on average by 40%, from stddev 0.06 to 0.1. The so distorted examples are fed back to each of the models and the error rates are displayed in the lower part of Table 4. The intriguing conclusion is that the adversarial examples remain hard for models trained even on a disjoint training set, although their effectiveness decreases considerably.

4.3 Spectral Analysis of Unstability

The previous section showed examples of deep networks resulting from purely supervised training which are unstable with respect to a peculiar form of small perturbations. Independently of their generalisation properties across networks and training sets, the adversarial examples show that there exist small additive perturbations of the input (in Euclidean sense) that produce large perturbations at the output of the last layer. This section describes a simple procedure to measure and control the additive stability of the network by measuring the spectrum of each rectified layer.

Mathematically, if $\phi(x)$ denotes the output of a network of K layers corresponding to input x and trained parameters W , we write

$$\phi(x) = \phi_K(\phi_{K-1}(\dots \phi_1(x; W_1); W_2) \dots; W_K),$$

where ϕ_k denotes the operator mapping layer $k-1$ to layer k . The unstability of $\phi(x)$ can be explained by inspecting the upper Lipschitz constant of each layer $k = 1 \dots K$, defined as the constant $L_k > 0$ such that

$$\forall x, r, \|\phi_k(x; W_k) - \phi_k(x + r; W_k)\| \leq L_k \|r\|.$$

The resulting network thus satsfies $\|\phi(x) - \phi(x + r)\| \leq L \|r\|$, with $L = \prod_{k=1}^K L_k$.

A half-rectified layer (both convolutional or fully connected) is defined by the mapping $\phi_k(x; W_k, b_k) = \max(0, W_k x + b_k)$. Let $\|W\|$ denote the operator norm of W (i.e., its largest singu-

Layer	Size	Stride	Upper bound
Conv. 1	$3 \times 11 \times 11 \times 96$	4	2.75
Conv. 2	$96 \times 5 \times 5 \times 256$	1	10
Conv. 3	$256 \times 3 \times 3 \times 384$	1	7
Conv. 4	$384 \times 3 \times 3 \times 384$	1	7.5
Conv. 5	$384 \times 3 \times 3 \times 256$	1	11
FC. 1	9216×4096	N/A	3.12
FC. 2	4096×4096	N/A	4
FC. 3	4096×1000	N/A	4

Table 5: Frame Bounds of each rectified layer of the network from [9].

lar value). Since the non-linearity $\rho(x) = \max(0, x)$ is contractive, i.e. satisfies $\|\rho(x) - \rho(x+r)\| \leq \|r\|$ for all x, r ; it follows that

$\|\phi_k(x; W_k) - \phi_k(x+r; W_k)\| = \|\max(0, W_k x + b_k) - \max(0, W_k(x+r) + b_k)\| \leq \|W_k r\| \leq \|W_k\| \|r\|$, and hence $L_k \leq \|W_k\|$. On the other hand, a max-pooling layer ϕ_k is contractive:

$$\forall x, r, \|\phi_k(x) - \phi_k(x+r)\| \leq \|r\|,$$

since its Jacobian is a projection onto a subset of the input coordinates and hence does not expand the gradients. Finally, if ϕ_k is a contrast-normalization layer

$$\phi_k(x) = \frac{x}{(\epsilon + \|x\|^2)^\gamma},$$

one can verify that

$$\forall x, r, \|\phi_k(x) - \phi_k(x+r)\| \leq \epsilon^{-\gamma} \|r\|$$

for $\gamma \in [0.5, 1]$, which corresponds to most common operating regimes.

It results that a conservative measure of the instability of the network can be obtained by simply computing the operator norm of each fully connected and convolutional layer. The fully connected case is trivial since the norm is directly given by the largest singular value of the fully connected matrix. Let us describe the convolutional case. If W denotes a generic 4-tensor, implementing a convolutional layer with C input features, D output features, support $N \times N$ and spatial stride Δ ,

$$Wx = \left\{ \sum_{c=1}^C x_c * w_{c,d}(n_1 \Delta, n_2 \Delta); d = 1 \dots, D \right\},$$

where x_c denotes the c -th input feature image, and $w_{c,d}$ is the spatial kernel corresponding to input feature c and output feature d , by applying Parseval's formula we obtain that its operator norm is given by

$$\|W\| = \sup_{\xi \in [0, N\Delta^{-1})^2} \|A(\xi)\|, \quad (1)$$

where $A(\xi)$ is a $D \times (C \cdot \Delta^2)$ matrix whose rows are

$$\forall d = 1 \dots D, A(\xi)_d = \left(\Delta^{-2} \widehat{w_{c,d}}(\xi + l \cdot N \cdot \Delta^{-1}); c = 1 \dots C, l = (0 \dots \Delta - 1)^2 \right),$$

and $\widehat{w_{c,d}}$ is the 2-D Fourier transform of $w_{c,d}$:

$$\widehat{w_{c,d}}(\xi) = \sum_{u \in [0, N)^2} w_{c,d}(u) e^{-2\pi i (u \cdot \xi) / N^2}.$$

Table 5 shows the upper Lipschitz bounds computed from the ImageNet deep convolutional network of [9], using (1). It shows that instabilities can appear as soon as in the first convolutional layer.

These results are consistent with the existence of blind spots constructed in the previous section, but they don't attempt to explain why these examples generalize across different hyperparameters or training sets. We emphasize that we compute upper bounds: large bounds do not automatically translate into existence of adversarial examples; however, small bounds guarantee that no such examples can appear. This suggests a simple regularization of the parameters, consisting in penalizing each upper Lipschitz bound, which might help improve the generalisation error of the networks.

5 Discussion

We demonstrated that deep neural networks have counter-intuitive properties both with respect to the semantic meaning of individual units and with respect to their discontinuities. The existence of the adversarial negatives appears to be in contradiction with the network’s ability to achieve high generalization performance. Indeed, if the network can generalize well, how can it be confused by these adversarial negatives, which are indistinguishable from the regular examples? Possible explanation is that the set of adversarial negatives is of extremely low probability, and thus is never (or rarely) observed in the test set, yet it is dense (much like the rational numbers), and so it is found near every virtually every test case. However, we don’t have a deep understanding of how often adversarial negatives appears, and thus this issue should be addressed in a future research.

References

- [1] David Baehrens, Timon Schroeter, Stefan Harmeling, Motoaki Kawanabe, Katja Hansen, and Klaus-Robert Müller. How to explain individual classification decisions. *The Journal of Machine Learning Research*, 99:1803–1831, 2010.
- [2] Yoshua Bengio. Learning deep architectures for ai. *Foundations and trends® in Machine Learning*, 2(1):1–127, 2009.
- [3] Jia Deng, Wei Dong, Richard Socher, Li-Jia Li, Kai Li, and Li Fei-Fei. Imagenet: A large-scale hierarchical image database. In *Computer Vision and Pattern Recognition, 2009. CVPR 2009. IEEE Conference on*, pages 248–255. IEEE, 2009.
- [4] Dumitru Erhan, Yoshua Bengio, Aaron Courville, and Pascal Vincent. Visualizing higher-layer features of a deep network. Technical Report 1341, University of Montreal, June 2009. Also presented at the ICML 2009 Workshop on Learning Feature Hierarchies, Montréal, Canada.
- [5] Pedro Felzenszwalb, David McAllester, and Deva Ramanan. A discriminatively trained, multiscale, deformable part model. In *Computer Vision and Pattern Recognition, 2008. CVPR 2008. IEEE Conference on*, pages 1–8. IEEE, 2008.
- [6] Ross Girshick, Jeff Donahue, Trevor Darrell, and Jitendra Malik. Rich feature hierarchies for accurate object detection and semantic segmentation. *arXiv preprint arXiv:1311.2524*, 2013.
- [7] Ian Goodfellow, Quoc Le, Andrew Saxe, Honglak Lee, and Andrew Y Ng. Measuring invariances in deep networks. *Advances in neural information processing systems*, 22:646–654, 2009.
- [8] Geoffrey E. Hinton, Li Deng, Dong Yu, George E. Dahl, Abdel rahman Mohamed, Navdeep Jaitly, Andrew Senior, Vincent Vanhoucke, Patrick Nguyen, Tara N. Sainath, and Brian Kingsbury. Deep neural networks for acoustic modeling in speech recognition: The shared views of four research groups. *IEEE Signal Process. Mag.*, 29(6):82–97, 2012.
- [9] Alex Krizhevsky, Ilya Sutskever, and Geoff Hinton. Imagenet classification with deep convolutional neural networks. In *Advances in Neural Information Processing Systems 25*, pages 1106–1114, 2012.
- [10] Quoc V Le, Marc’Aurelio Ranzato, Rajat Monga, Matthieu Devin, Kai Chen, Greg S Corrado, Jeff Dean, and Andrew Y Ng. Building high-level features using large scale unsupervised learning. *arXiv preprint arXiv:1112.6209*, 2011.
- [11] Yann LeCun and Corinna Cortes. The mnist database of handwritten digits, 1998.
- [12] Tomas Mikolov, Kai Chen, Greg Corrado, and Jeffrey Dean. Efficient estimation of word representations in vector space. *arXiv preprint arXiv:1301.3781*, 2013.
- [13] Matthew D Zeiler and Rob Fergus. Visualizing and understanding convolutional neural networks. *arXiv preprint arXiv:1311.2901*, 2013.